Astron. Astrophys. 336, 637–647 (1998)

ASTRONOMY AND ASTROPHYSICS

High resolution spectroscopy of symbiotic stars⋆

IV. BX Monocerotis: orbital and stellar parameters

T. Dumm[1], **U. Mürset**[1], **H. Nussbaumer**[1], **H. Schild**[1], **H.M. Schmid**[2], **W. Schmutz**[1], **and S.N. Shore**[3]

[1] Institut für Astronomie, ETH-Zentrum, CH-8092 Zürich, Switzerland
[2] Landessternwarte Heidelberg-Königstuhl, D-69117 Heidelberg, Germany
[3] Department of Physics and Astronomy, Indiana University South Bend, 1700 Mishawaka Avenue, South Bend, IN 46634-7111, USA

Received 22 April 1998 / Accepted 19 May 1998

Abstract. We investigate the orbit and the components of the symbiotic BX Mon system with new high resolution spectroscopy, IUE spectra, published photographic magnitudes, and brightness estimates from the RASNZ. We review the available photometry and deduce a new binary period of $1401\ \mathrm{days}$. We also find evidence in the IUE data that BX Mon is an eclipsing system.

With our high resolution spectroscopy we determine the radial velocity curve of the M giant from photospheric absorption features. BX Mon is unusual for a symbiotic star in that its hot component is also observable in the optical wavelength region. From corresponding absorption features we are able to measure the hot component's radial velocity. We determine semi–amplitudes for the cool and the hot components of 4.3 $\mathrm{km\,s^{-1}}$ and 29 $\mathrm{km\,s^{-1}}$, respectively. The mass ratio is thus ~ 7 which is among the highest yet found for symbiotic systems.

The orbit of BX Mon is eccentric with an ellipticity of $e = 0.49$. The binary mass function is $0.0076\,\mathrm{M}_\odot$. We determine the mass of the red giant as $M_\mathrm{r} = 3.7\,\mathrm{M}_\odot$ and the mass of the hot component as $M_\mathrm{h} = 0.55\,\mathrm{M}_\odot$. This low M_h suggests that even relatively high mass symbiotics are unlikely to be supernova Type I progenitors.

The distance to BX Mon of $3\ \mathrm{kpc}$ is determined with the Na I $\lambda\lambda 5890, 5896$ interstellar absorption lines and the interstellar extinction feature at 2200 Å. For the luminosity of the cool component we find $L_\mathrm{r} = 3400\ \mathrm{L}_\odot$ and a stellar radius $R_\mathrm{r} = 160\ \mathrm{R}_\odot$. The red giant's radius remains within the inner Lagrangian point, even at periastron. The hot component is unlikely to be a main sequence star.

Key words: binaries: eclipsing – binaries: symbiotic – stars: fundamental parameters – stars: individual: BX Mon

Send offprint requests to: T. Dumm

⋆ Based on observations obtained at the European Southern Observatory, La Silla (Chile), visual brightness data from the RASNZ, and UV spectra from the IUE archive. ESO observations were granted for the programs 47.7-081, 48.7-083, 49.7-041, 50.7-129, 51.7-093, 52.7-068, 53.7-083, 54.E-061, 55.E-446, 56.E-526

1. Introduction

Stars with combination spectra are those whose spectra show simultaneously very high excitation emission lines and low temperature absorption features, but which cannot be considered certain binaries. Some or all may, however, be so. Under this heading BX Mon entered Bidelman's (1954) list of 'combination stars' – which was at that time the designation for what we call symbiotic systems. Due to the low degree of excitation in the optical emission lines BX Mon was excluded from Allen's (1979, 1982) catalogs of symbiotic stars. The presence of medium ionized species became evident with the International Ultraviolet Explorer (IUE) spectra of Michalitsianos et al. (1982). Observed emission features in the UV are C III], C IV, N III], and O III]. This property was most likely the reason for the inclusion in Allen's (1984) catalog.

BX Mon is an unusual symbiotic system in the sense that its hot component is rather cool and easily detected in the long wavelength IUE and blue optical spectra. Michalitsianos et al. (1982) remarked on the strong continuum in the long wavelength range of IUE, which they described as resembling that of a late A to early F star.

Photographic monitoring of BX Mon from 1890 to 1940 revealed a periodicity of 1380 days and an amplitude of about 3 magnitudes (Mayall 1940). This was often interpreted as due to a very long period Mira variable, and it entered, under this flag, the General Catalog of Variable Stars (Kukarkin et al. 1958). Later Whitelock & Catchpole (1983) suggested that the infrared spectrum and colours are appropriate for a normal $\sim$ M5 giant and not for a Mira variable. This is supported by the published *K*-magnitudes for BX Mon which give a mean value of $K = 5.7$ with a 1σ-scatter of $0.1\ \mathrm{mag}$ (Whitelock & Catchpole 1983; Viotti et al. 1986; Kenyon 1988; Munari et al. 1992). These IR data and the extensive spectroscopic monitoring by Iijima (1985) established that the periodic variations are caused by the change of the viewing angle due to orbital motion.

In this Paper, we present radial velocity measurements which provide orbital information for the BX Mon system. We re-examine photometric data in order to establish the orbital period. We determine the binary mass-ratio and the masses of the individual components. The distance to BX Mon is esti-

Table 1. Log of our ESO high resolution spectroscopy of BX Mon redwards of 6000 Å. We give the orbital phase ϕ (Eq. 1), the central wavelength λ_c, the heliocentric radial velocity derived from absorption lines, v_r, the Hα emission line equivalent width, EW(Hα) and the line flux I(Hα) (in scaled units, see Sect. 7.1).

Date	ϕ	λ_c [Å]	v_r [km s^{-1}]	EW(Hα) [Å]	I(Hα)
1988, Dec 14[1)]	0.56	6563	28.0 ± 1.0	46	
1991, Sep 12	0.27	6563	[2)]	[2)]	
1991, Oct 22	0.30	6563	[2)]	41	82
1992, Jan 3	0.35	6563	28.2 ± 1.0	52	56
1992, Jan 4	0.35	7005	29.1 ± 0.7		
1992, Mar 17	0.41	6563	27.7 ± 1.0	28	36
1992, Mar 18	0.41	7005	27.2 ± 0.7		
1993, Jan 15	0.62	6563	26.1 ± 1.0	37	34
1993, Jan 16	0.62	7005	26.9 ± 0.7		
1993, Feb 20	0.65	6563	[2)]	47	33
1993, Feb 21	0.65	7005	27.2 ± 0.7		
1993, Oct 29	0.83	6563	28.2 ± 1.0	39	35
1993, Oct 30	0.83	7005	28.1 ± 0.7		
1994, Jan 11	0.88	6563	[2)]	39	29
1994, Jan 15	0.88	7005	27.4 ± 0.7		
1994, May 13	0.97	6563	30.7 ± 1.0	8	8
1994, Oct 31	0.09	7005	35.5 ± 0.7		
1994, Nov 1	0.09	6563	[2)]	68	90
1995, Jan 5	0.14	7453	34.2 ± 0.5		
1995, Jan 6	0.14	7453	33.9 ± 0.5		
1995, Apr 2	0.20	7453	31.2 ± 0.5		
1995, Apr 3	0.20	6563	[2)]	62	70
1995, Sep 14	0.32	7453	27.6 ± 0.5		
1996, Mar 5	0.44	7453	26.9 ± 0.5		

[1)] Observation from Van Winckel et al. (1993) [2)] Low signal to noise

Table 2. Log of our ESO high resolution observations of BX Mon bluewards of 6000 Å. We give the orbital phase ϕ (Eq. 1), the central wavelength λ_c and the heliocentric radial velocities from cross-correlation with an A-star spectrum, v_h, and with an M-star spectrum, v_r.

Date	ϕ	λ_c [Å]	v_h [km s^{-1}]	v_r [km s^{-1}]
1988, Oct 21[1)]	0.52	5007	[2)]	28.7 ± 1.0
1993, Nov 1	0.83	5880	[2)]	28.7 ± 1.0
1995, Jan 7	0.14	4686	[2)]	32.1 ± 2.0
1996, Mar 6	0.44	4070	40.8 ± 3.0	27.2 ± 2.0
1996, Mar 31	0.46	4363	42.8 ± 3.0	28.6 ± 3.0
1997, Jan 18	0.67	4070	[2)]	29.6 ± 2.0
1997, Feb 20	0.69	4070	[2)]	29.8 ± 2.0
1997, Mar 7	0.70	4070	[2)]	31.4 ± 2.0

[1)] Observation from Van Winckel et al. (1993)
[2)] No measurable absorption lines from the hot component

Table 3. Log of IUE spectra of BX Mon. We give the orbital phase (Eq. 1), archive number, FES-magnitude and the integrated observed flux in [10^{-12}erg cm^{-2}s^{-1}] in the two intervals I_S from 1800 to 1880 Å and I_L from 3010 to 3090 Å , which are free of strong emission lines.

Date	ϕ	SWP	LWR/P	FES	I_S	I_L
1979, Jan 6	0.97	03832L	03408L	11.0	0.2	2.1
1979, Sep 1	0.14	06344L	05479L	11.0	1.3	5.3
1986, Feb 26	0.83	27797L	07724L	10.8	1.9	10.3
1989, Mar 14	0.62	35767L	15196L	11.1	2.1	5.8
1990, Dec 1	0.07	40243L	-	11.9	0.2	-
1995, Oct 27	0.35	56128L	-	[1)]	1.7	-
1995, Oct 28	0.35	56132L	31630L	[1)]	1.9	5.8

[1)] No reliable FES value available (scattered light)

mated with the help of interstellar absorption lines as well as from interstellar extinction. This enables the calculation of stellar parameters like luminosity and radius. We then measure and discuss the rotation of the cool component and present a series of Hα line profiles. We finally consider a model in which the variability of the Hα line can be understood.

2. Spectroscopic data

2.1. Optical and near IR spectroscopy

We have monitored BX Mon regularly with the CAT 1.4 m telescope and the Coudé Echelle spectrograph (CES) at the ESO observatory at La Silla, Chile. The observations were carried out remotely from Garching, Germany. The optical spectra were taken with a resolution $R = 60\,000$ and cover a spectral interval of 60 Å. Spectra centered at 7453 Å have a resolution $R = 100\,000$ and cover 50 Å. We complement our data with observations by van Winckel et al. (1993) who used the same telescope and instrument. A log of our optical observations is given in Table 1 and Table 2. The details of the CAT observations and data reduction are as described in Schmid et al. (1998, Paper III).

For the purpose of spectral classification we took a near IR spectrum with $R = 2\,000$, covering the range 6 800 Å – 10 700 Å on March 15, 1992 with the ESO 1.5 m telescope. For a description of this observation see Mürset & Schmid (1998).

2.2. UV data

We retrieved all the available low resolution IUE spectra of BX Mon from the final IUE archive. A log of the IUE observations is given in Table 3. The last entry in Table 3 refers to an observation, that suffered from scattered light caused by a problem with the IUE optics. The spectrum was corrected with the LWP 31623L sky exposure. No high resolution spectra of BX Mon have been taken by IUE.

3. The orbital period

Our radial velocity data are not suited for a good period determination. They are, however, compatible with the 1380 day periodicity found by Mayall (1940). The precision of Mayall's period

was put into question by the work of Iijima (1985). Although he found the same periodicity, his interpretation of spectroscopic changes as periodic attenuation by the cool giant was inconsistent with Mayall's ephemeris $\mathrm{Max.} = \mathrm{J.D.}\,2412490 + 1380^d \times E$ in the sense that his minimum phase was shifted by about half a period with respect to that of Mayall. Because the period is of prime importance in our study and accurate periods can only be obtained from data with a long time base we re-determine the periodicity of the light variations from the available data.

3.1. The light curve of BX Mon

For our analysis of the light variations of BX Mon we employed two data sets.

The first set consists of the original data from Mayall's laboratory journal kindly provided by The Harvard College. These brightness estimates are based on photographic plates and cover the period from 1890 to 1940 (see Mayall 1940). The dataset consists of 731 detections. The error of a measurement is ± 0.3 magnitudes and the amplitude of the variations amounts to ≈ 3 magnitudes.

The second data set has been kindly provided by the Royal Astronomical Society of New Zealand (RASNZ). It consists of the visual brightness estimates reported on a regular basis by the variable star section of the RASNZ. These data cover the years 1989 to 1995.

Although separated by more than half a century both light curves are similar (Fig. 1c,d). They show a relatively narrow maximum and a wide flat minimum with approximately the same periodicity.

A period analysis applied to the combined data sets yields two possible periodicities, $P = 1338 \pm 8$ days and $P = 1401 \pm 8$ days. Our analysis excludes Mayall's period of 1380 days because the maxima of the old (Mayall) and the new light curves (RASNZ) are out of phase by about half a period. As mentioned above, this problem was already encountered by Iijima (1985). A reanalysis of Mayall's data alone confirms the 1380 day period, but the uncertainty is rather large and includes the two periods determined by us with the combined data set.

The ambiguity in the orbital period can be resolved if we include the IUE data into the analysis and examine the UV eclipse behaviour.

3.2. Eclipse effects in the UV

The complete set of IUE archive data is shown in Fig. 2. In two IUE measurements we see a strong flux attenuation (Table3) which can be interpreted as eclipses of the hot component by the cool giant. The two observations are separated by 4347 days or a little more than 3 periods. We compared phase plots of the integrated IUE fluxes from $1800-1880$ Å and $3010-3090$ Å for $P = 1338 \pm 8$ days and $P = 1401 \pm 8$ days. Using $P = 1338 \pm 8$ days puts an IUE spectrum with high flux level between the two IUE spectra with strongly reduced integrated fluxes. This behavior is not consistent with an eclipse interpretation of the IUE flux reduction. Only an orbital period of $P = 1401 \pm 8$ days

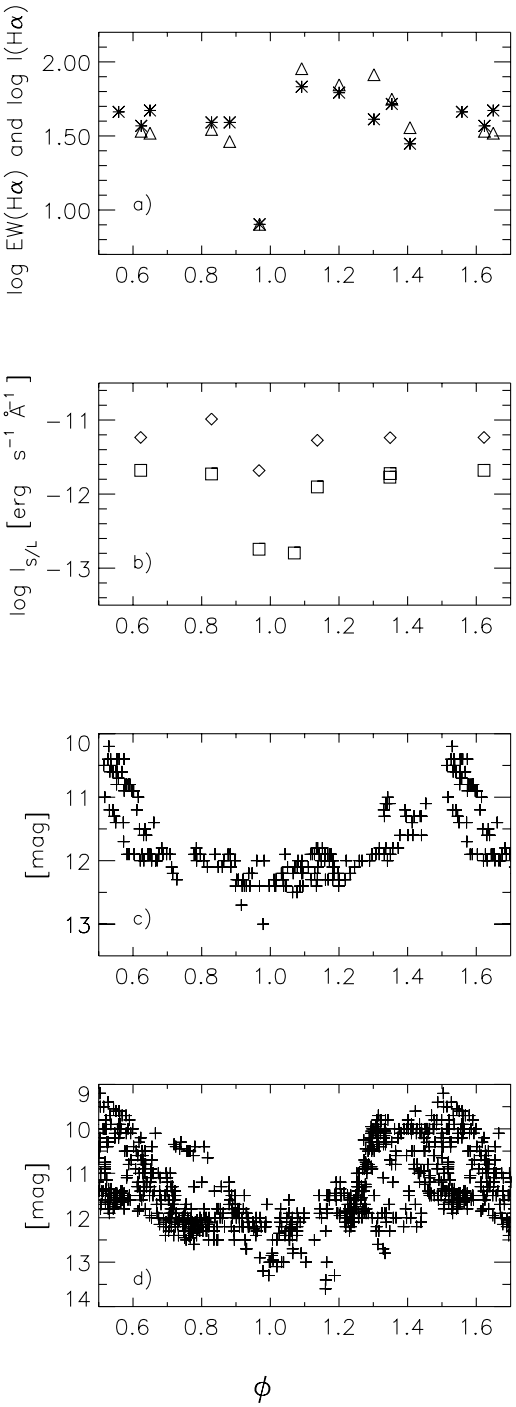

Fig. 1a–d. Phase plot of **a** Hα equivalent widths (asterixes) and Hα line fluxes (triangles), **b** integrated IUE continua around 1840 Å (squares) and 3050 Å (diamonds), **c** visual magnitudes of RASNZ and **d** Mayall's photographic magnitudes.

is consistent with an eclipsing system as shown in Fig. 1a,b). This interpretation implies, that the eclipse phase lasts in the far UV for about 150 days. Such long UV-eclipses, about 10% of the orbital period, are characteristic for symbiotic systems. Our eclipse interpretation is also strongly supported by the measured

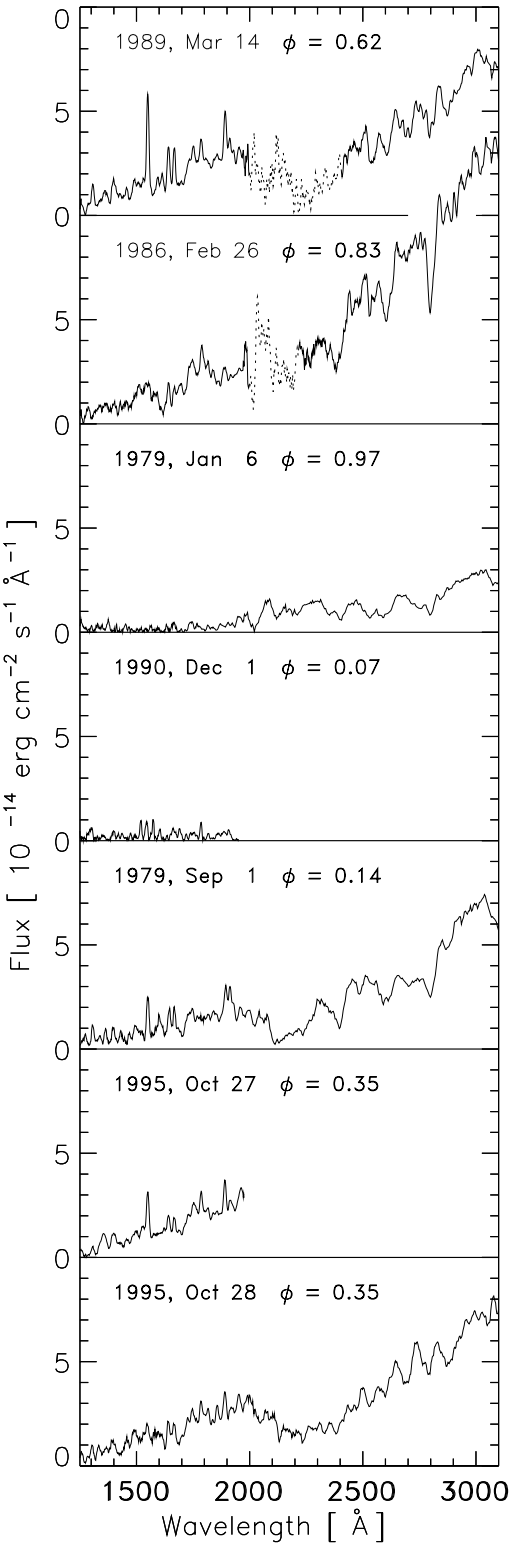

Fig. 2. BX Mon IUE spectra, smoothed with a 7 point running box. The spectral intervals that show merely noise are marked with a dotted line.

radial velocities (see Sect. 4.1). Throughout this paper we will use the period $P = 1401 \pm 8$ days .

4. Radial velocity curves and stellar masses

Initially we had taken high resolution data only in the red spectral range $\lambda > 6000$ Å in order to determine a radial velocity curve for the cool giant (Table 1). It turned out that our data disagreed with those of Garcia (1986) when interpreted as orbital motion of the cool giant. In fact Garcia's measurements are compatible with an opposite radial velocity curve, as expected for a companion in a double lined spectroscopic binary. Garcia's (1986) measurements were centered at 5200 Å, where the hot component could contribute significantly to the spectrum. Subsequently, we succeeded on two occasions to measure the radial velocity of the hot component from absorptions in the blue spectral range (Table 2). In the following we discuss the radial velocity data for the hot and cool component separately.

4.1. Radial velocity curve of the M star

To derive the orbital parameters of the cool giant we use only observations in the red and near IR ($\lambda > 6000$ Å). For these wavelengths we can safely assume that the absorption lines of the red giant are not significantly disturbed by the A-type spectrum of the hot star. The radial velocity of the red star in BX Mon was determined by cross-correlating observations of the symbiotic star with the radial velocity standard HD 108 903. The radial velocity curve analysis was done in the same way as described in Schmutz et al. (1994, Paper I). For the velocity standard we adopt a radial velocity of $21.3 \pm 0.3\ \mathrm{km\,s^{-1}}$ from the Astronomical Almanac (1994). Because of the weak continuum in some of the 6563 Å settings, not all of these spectra are suited for radial velocity determinations.

In order to find the orbital parameters: time of periastron passage, T_P, systemic velocity, V_0, radial velocity semi-amplitude, K_r, eccentricity, e and position angle, ω we have performed a least squares fit. For this we used a fixed period of $P = 1401$ days as derived in the previous section. The best fit parameters are listed in Table 4 and the corresponding radial velocity curve is shown in Fig. 3. The radial velocity solution predicts the red star in front of the hot component at

$$\mathrm{mideclipse} = 2\,449\,530 + 1401 \cdot E. \quad (1)$$

This is consistent with the reduced flux in the IUE spectra taken on Jan. 6, 1979 and Dec. 1, 1990. The red giant eclipses the hot component at $\phi = 0.00$, periastron passage takes place at phase $\phi = 0.10$, the hot component is in front of the red star at $\phi = 0.20$ and the apastron is at $\phi = 0.60$.

4.2. Radial velocities for the hot component

Since the spectrum of the hot component stretches well into the visible spectral range it is, in principle, amenable to radial velocity observations with high spectral resolution. We have compared the BX Mon spectra taken below 6000 Å with that of M-giants and A-supergiants. In two spectra from March 1996 we detected absorption lines, that we attribute to the atmosphere of the hot component. In the spectrum centered at 4070Å taken

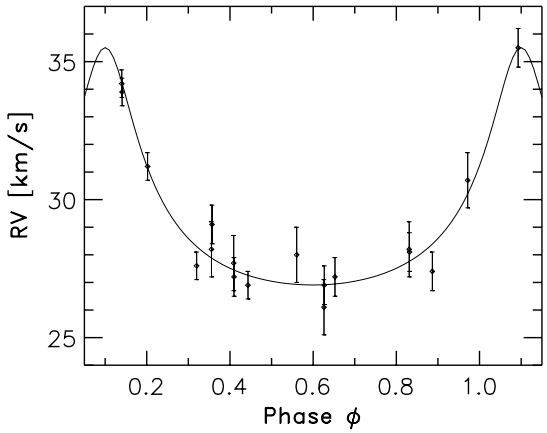

Fig. 3. Radial velocity of the M5 III star in BX Mon based on observations centered redwards of 6000 Å

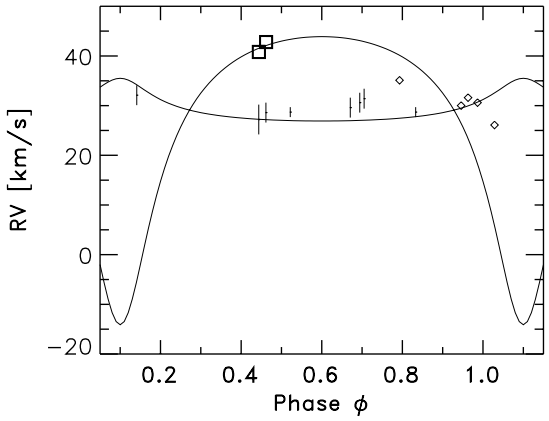

Fig. 4. Radial velocity curve of the hot and cool components. The symbols represent our two radial velocity measurements of the hot component (squares), the radial velocity measurements of the M-star derived from spectra centered blueward of 6000 Å (vertical lines) and Garcia's (1986) radial velocity values derived from spectra centered at 5300Å (diamonds).

Table 4. Orbital parameters of the M star in BX Mon, assuming $P = 1401$ days. T_0 gives the Julian date at which the cool star is in front of the hot component, T_P gives the time of periastron passage.

Parameter	Best solution	Uncertainty
T_0 [JD]	2 449 530	± 60
T_P [JD]	2 449 667	± 20
V_0 [km s^{-1}]	29.1	± 0.8
K_r [km s^{-1}]	4.3	± 0.3
e	0.49	± 0.05
ω [°]	0	± 10
$\sigma(O-C)$ [km s^{-1}]	0.6	

at phase $\phi = 0.44$ and the spectrum centered at 4363Å taken at phase $\phi = 0.46$ we see that at wavelengths at which A-stars have strong absorption lines, the spectrum of an M-standard does not fit well the spectrum of BX Mon. In these two spectra we also have to assume an additional continuum contribution in order to scale the BX Mon spectrum to that of the comparison M-star. In these two observations we are thus seeing a superposition of the M-star spectrum and an A-star spectrum caused by the hot component. These observations allow us to determine radial velocities for the red and the hot component in BX Mon. Cross-correlation with a M3III and an A8Ia star leads to the radial velocity values listed in Table 2.

The two values in Table 2 for the hot component, were used to determine the radial velocity semi-amplitude of the hot component K_h. We employed the parameters V_0, e, and T_P as determined for the red giant. We set $\omega = 180°$. The only parameter we have to fit is thus K_h. As shown in Fig. 4, we find

$$K_\mathrm{h} = 29 \pm 5 \ \mathrm{km\,s^{-1}}. \quad (2)$$

Further measurements at phases when the system is bright in the optical are needed to improve the accuracy of our result. Unfortunately, Garcia's (1986) measurements do not improve the accuracy of the K_h-determination. As both components may contribute to the spectrum, his cross-correlations may suffer from a blending effect. This would explain his values which lie between our radial velocity curves In fact, our measurements of the red star velocity from settings at wavelengths < 6000Å also differ from the solution derived in Sect. 4.1, but we cannot derive additional radial velocities of the hot component from these settings.

4.3. Mass function and stellar masses

We determine first the binary mass function based on the well defined radial velocity curve of the red giant. The mass function is defined as

$$f(m) = \frac{1}{2\pi G} \cdot P K_\mathrm{r}^3 (1-e^2)^{3/2} = \frac{(M_\mathrm{h} \sin i)^3}{(M_\mathrm{h} + M_\mathrm{r})^2} \quad (3)$$

where M_h and M_r stand for the masses of the hot star and the red giant, i for the orbital inclination, P for the period, K_r for the radial velocity semi-amplitude of the red star, and G for the gravitational constant. The values from Table 4 yield for the BX Mon system.

$$f(m) = 0.0076 \pm 0.0022 \ \mathrm{M_\odot} \ . \quad (4)$$

To derive stellar masses we need in addition the mass ratio and the orbital inclination. From the radial velocity amplitude we obtain a mass ratio of

$$q = \frac{K_\mathrm{h}}{K_\mathrm{r}} = \frac{M_\mathrm{r}}{M_\mathrm{h}} = 6.7 \pm 1.3. \quad (5)$$

For the inclination we can determine a lower limit from the observed eclipse in the UV. The radius as derived in Sect. 6.2 together with the binary separation at eclipse calculated with the upper limit $\sin i = 1$ leads to an inclination $\sin i = 0.94 \pm 0.06$ which corresponds to a lower limit of $i \geq 62°$ for the inclination.

We can thus determine both stellar masses according to

$$M_\mathrm{h} = \frac{(1+q)^2 \cdot f(m)}{\sin^3 i} = 0.55 \pm 0.26 \ \mathrm{M_\odot} \quad (6)$$

Table 5. Summary of newly derived parameters for the BX Mon system.

	Adopted value	Error ±
Orbit:		
Period P [days]	1401	8
Eccentricity e	0.49	0.05
Inclination $\sin i$	0.94	0.06
Semi-major axis a [AU]	4.0	0.7
Periastron distance red star – L_1 [AU]	1.1	
Red giant:		
Mass M_r [$M_\odot$]	3.7	1.9
Radius R_r [$R_\odot$]	160	50
Luminosity L_r [$L_\odot$]	3400	1700
Spectral type	M5	1
Effective temperature [K]	3470	200
Rotational velocity $v \sin i$ [km s^{-1}]	8.5	1.5
Hot component:		
Mass M_h [$M_\odot$]	0.55	0.26
System parameters:		
Distance d [pc]	3000	750
Total mass M_tot [$M_\odot$]	4.3	1.9

$$M_\mathrm{r} = q \cdot M_\mathrm{h} = 3.7 \pm 1.9\ \mathrm{M}_\odot. \quad (7)$$

The above mass M_h is typical for a white dwarf. Hot components with similar mass values have indeed been found in other symbiotic systems (Mikolajewska & Kenyon 1992, Schmutz et al. 1994, Schild et al. 1995) The mass-ratio and the total system mass $M_\mathrm{tot} = 4.3 \pm 1.9\,M_\odot$ are slightly higher than for most other symbiotics (Mikolajewska 1997, Schmid 1998).

All newly derived orbital and stellar parameters of the BX Mon system are summarized in Table 5 and the orbits of the two components are illustrated in Fig. 5. The separation between the two components varies between 2.0 and 5.9 AU. At periastron the inner Lagrangian point L_1 is at 1.1 AU, that is 1.6 times the radius of the cool component. Thus even at periastron, L_1 is well detached from the red giant.

5. Distance to BX Mon

The interstellar Na I $\lambda\lambda 5889.95, 5895.92$ absorption lines which we observed at high spectral resolution allow us to derive a lower limit for the distance to BX Mon. Nulling the absorption feature at 2200 Å in the IUE low resolution data yields A_V, which puts an upper limit on the distance.

5.1. Interstellar absorption lines

The galactic coordinates of BX Mon are $l^{II} = 220.04°$, $b^{II} = +5.88°$. The velocity structure of the interstellar medium has been studied in detail by Brand & Blitz (1993). In the direction of BX Mon, the radial velocity of the interstellar Na I D lines is increasing with increasing distance. The Na I doublet in the spectra of BX Mon, shows a complex signature (see Fig. 6). As both components show the same structure, we can assume that the observed profiles are real, without significant noise. The radial velocities of the cool and of the hot component at the time of observation are $v_\mathrm{c} = 12$ km s^{-1} and $v_\mathrm{h} = 18$ km s^{-1} in the local standard of rest (LSR). Na I absorptions with radial velocities larger than these values are thus most probably caused by the interstellar medium. According to Brand & Blitz (1993), the strong absorption feature corresponding to $v_\mathrm{LSR} \sim 40$ km s^{-1} indicates a distance of ~ 3000 pc. The weak absorption feature at $v_\mathrm{LSR} \sim 50$ km s^{-1} would be associated with interstellar clouds at 3500 pc. We therefore use the 3000 pc as a lower limit for the distance to BX Mon.

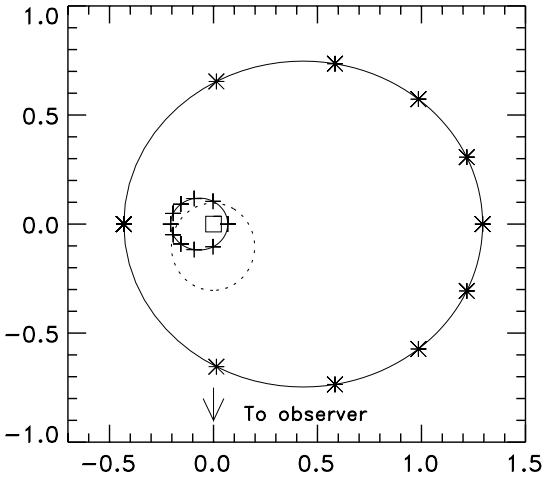

Fig. 5. Orbit of the red giant (+) and hot component (*) in the BX Mon system in steps of $\Delta\phi = 0.1$. In this representation, the stars move anti-clockwise. The dotted circle represents the red giant boundary at $\phi = 0$. The square marks the center of gravity. Axes are in units of the semi-major axis a.

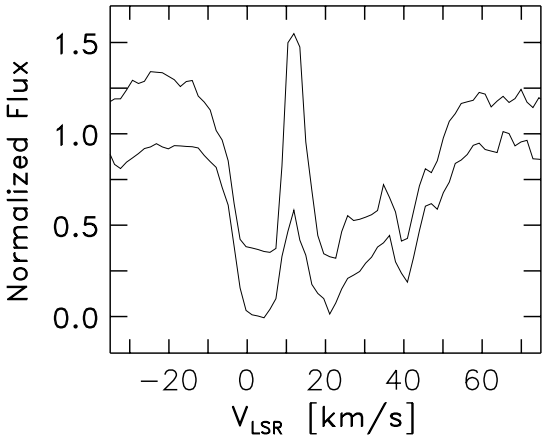

Fig. 6. Interstellar absorption lines Na I λ 5890 (top, shifted by +0.25) and Na I λ 5896 (bottom) in the spectrum of Nov 1, 1993, transformed into the local standard of rest (LSR).

5.2. Interstellar reddening

The better exposed IUE spectra of BX Mon show the broad 2200 Å feature which can be used to determine the interstellar extinction. As the UV-continuum emission of BX Mon is similar to that of a late A or early F type star, which in itself has some spectral structure at 2200 Å, it is not advisable to simply straighten the spectrum to a steadily increasing continuum because that would tend to overestimate the extinction value. Instead we derive $E_{\rm B-V}$, using the mean interstellar extinction law of Seaton (1979), by comparing the BX Mon spectra with that of a spectral standard of known extinction. The spectral standard HD 59 612 fits the absorption line spectrum of BX Mon well in the UV. Fanelli et al. (1992) find for this A5I star $E_{\rm B-V} = 0.14$. For BX Mon we obtain $E_{\rm B-V} = 0.25 \pm 0.05$, which agrees with earlier estimates by Viotti et al. (1986). Assuming $R = A_{\rm V}/E_{\rm B-V} = 3.1$ and using $A_\lambda/E_{\rm B-V}$ as tabulated in Savage & Mathis (1979) leads to $A_{\rm V} = 0.8 \pm 0.2$, $A_{\rm J} = 0.22 \pm 0.04$ and $A_{\rm K} = 0.10 \pm 0.02$.

Neckel & Klare (1980) have examined the spatial distribution of the interstellar extinction. Field 69 and 70 which are close to BX Mon can be used to estimate an upper limit for the distance of BX Mon. At a distance of 3000 pc, there is a steep increase in $A_{\rm V}$ from $A_{\rm V} \sim 1$ to much higher values, making this value an upper limit for the distance. Together with the interstellar Na I absorption features we thus estimate the distance of BX Mon to be

$$d = 3000 \pm 750 \ {\rm pc} \tag{8}$$

6. The red giant

6.1. Effective temperature

We compared our BX Mon low resolution near IR spectrum spectrum with spectral standards. This leads to a spectral type M5.0 ± 0.5 with no definite luminosity classification. Iijima (1985) determined the spectral type to be M5 – M6. Viotti et al. (1986) classified it as M6$\pm$1 III with some uncertainty in the luminosity class. Schulte-Ladbeck (1988) finds a spectral type M4 with no luminosity classification. For the rest of this paper, we adopt a spectral type of M5 ± 1. The effective temperature scale for late giants from Dyck et al. (1996) yields an effective temperature $T_{\rm eff} = 3470 \pm 200$ K.

6.2. Radius and luminosity

We determine the radius of the M-star in BX Mon with the *K* magnitude, the $(J-K)$-colour and the distance. *J* and *K* magnitudes are given in Whitelock & Catchpole (1983), Viotti et al. (1986) and Munari et al. (1992). They vary only very slightly with a 1σ-scatter of 0.1 mag and are consistent with no light variations of the red giant. We use the average $J = 7.0 \pm 0.1$ and $K = 5.7 \pm 0.1$ or de-reddened $J_0 = 6.8 \pm 0.1$ and $K_0 = 5.6 \pm 0.1$. Taking the surface brightness relation $F_{\rm K}$ for M-giants given in Schild et al. (1998), we find a M-star radius:

$$R_{\rm r} = d \cdot 10^{2.70-0.2\ K+0.13\ (J-K)} = 160 \pm 50\ {\rm R}_\odot, \tag{9}$$

where d is the distance in kpc. According to Dumm & Schild (1998) this radius is typical for a star with this spectral type and mass. Together with the effective temperature, this leads to a luminosity $L_{\rm r} = 3400 \pm 1700\ {\rm L}_\odot$.

With our luminosity $L_{\rm r}$ and effective temperature $T_{\rm eff}$ we estimate a red giant mass from evolutionary tracks. RGB and AGB evolutionary tracks for stars of more than $M_{\rm r} = 1.5\ {\rm M}_\odot$ coincide. Taking the $M_{\rm bol}$ versus $T_{\rm eff}$ diagram of RGB and AGB models by Bessell et al. (1989) leads to $M_{\rm r} = 3 \pm 2\ {\rm M}_\odot$. This is consistent with the value derived from the radial velocity curves.

6.3. Stellar rotation

Single M giant stars are expected to have negligible rotation velocities, due to their large moment of inertia. In Fig. 7 the spectrum of a M5 III star, shows considerably narrower absorption lines than BX Mon. The additional line broadening is understood in terms of a rotating M-star in BX Mon, expected as a consequence of binary tidal forces. Stellar rotation analysis methods can be split into those based on stellar disk integration methods and those using convolution techniques. The convolution method is identical to the disk integration method if line-broadening is constant over the whole stellar surface. For late type stars, Marcy & Chen (1992) have compared calculated line profiles using convolution techniques with those calculated by disk integration. They find that for M stars with projected rotational velocities as small as $v \sin i = 2\ {\rm km\,s^{-1}}$, the two methods lead to the same line profiles with a precision of 5 percent, therefore we make use of the simpler convolution methods.

We derive the rotational velocity of the M star by comparing its absorption lines with those of spectral standards which are believed to be single stars. We assume that the line broadening is only a function of spectral subtype. We can then use the non-rotating spectral standards as a template. We find, that the line widths in our M4 III and M5 III spectral standards are identical with a precision of $v \sin i \leq 1\ {\rm km\,s^{-1}}$.

As pressure broadening is much smaller than micro-turbulence, and macro-turbulence broadening in M-giants, we do not expect to introduce significant errors by employing non-rotating reference stars of different masses. The uncertainty in the spectral type of BX Mon is expected to introduce an error $\Delta v \sin i \leq 1.0\ {\rm km\,s^{-1}}$. The line-broadening in BX Mon can then be written as:

$$F_{\rm BX\ Mon}(\lambda) = R(\lambda) * F_{\rm M5\ III}(\lambda) \tag{10}$$

where R stands for the rotational broadening function which depends only on $v \sin i$ and limb-darkening which is approximated by a linear darkening, with limb darkening coefficient 0.6, Gray (1992). $F_{\rm M5III}$ stands for the line profile of the non-rotating M5 III-spectral standard and $F_{\rm BX\ Mon}$ for the measured

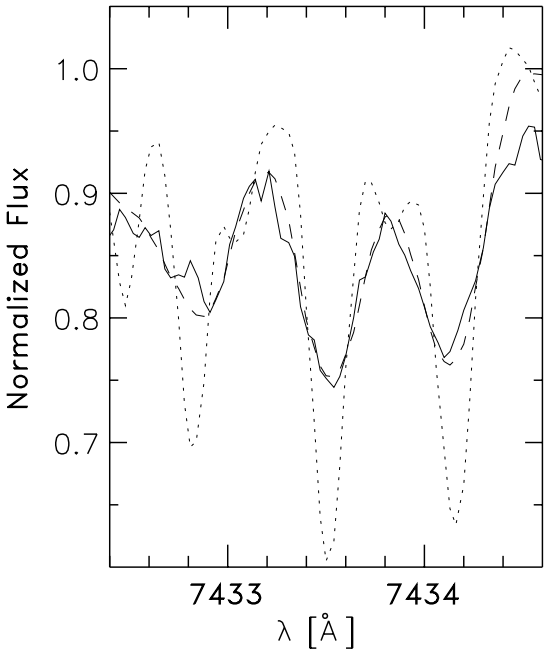

Fig. 7. High resolution spectrum of BX Mon (solid), a standard M5 III spectrum (dotted) and the M5 III spectrum convolved with the rotational broadening function corresponding to $v \sin i = 9 \mathrm{km\,s^{-1}}$ (dashed).

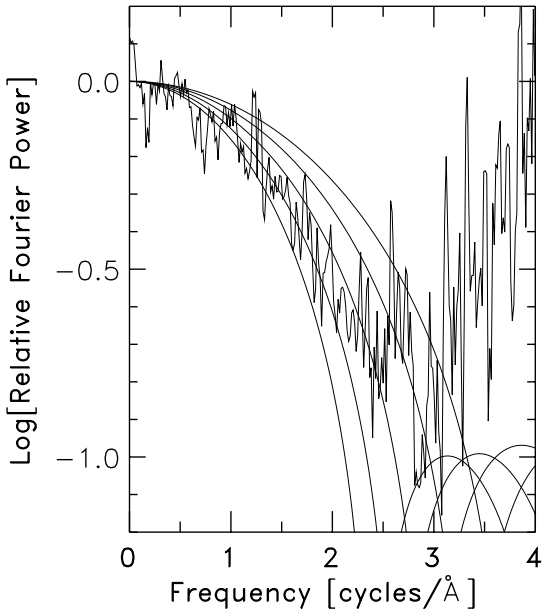

Fig. 8. Ratio of Fourier transform of BX Mon and of the M5 III spectral standard. Overlayed are Fourier transforms of the rotational broadening function belonging to the values $v \sin i = 7, 8, 9, 10, 11 \ \mathrm{km\,s^{-1}}$.

line profile in BX Mon. After Fourier transformation this equation can be written as :

$$f_{\mathrm{BX\ Mon}}(\sigma) = r(\sigma) \cdot f_{\mathrm{M5\ III}}(\sigma) \tag{11}$$

or, when solved for $\log[r(\sigma)]$,

$$\log[r(\sigma)] = \log[f_{\mathrm{BX\ Mon}}(\sigma)] - \log[f_{\mathrm{M5\ III}}(\sigma)] \tag{12}$$

We determine the rotation velocity in two ways. First we convolve the non-rotating star with the rotational broadening function belonging to various $v \sin i$. According to Tsuji et al. (1994), measurable saturation effects are expected for absorption lines stronger than 0.80 relative to a continuum normalized to 1. We have therefore chosen an interval containing weak lines, which are expected to show little or no saturation effects. The rotation velocity, that leads to the best fit is $v \sin i = 9 \pm 3 \ \mathrm{km\,s^{-1}}$ (see Fig. 7).

The second method, which is described in detail in Marcy & Chen (1992) and Gray (1992), fits the Fourier transform of the rotational broadening function to the ratio of the Fourier transforms of the spectra of BX Mon and the spectral standard. The spectrum employed for this procedure covers the range $7425 - 7475$ Å. By choosing a large spectral interval, we reduce the effect of the imperfect normalization on the Fourier transform. The result of this procedure is shown in Fig. 8. At frequencies above ~ 2.5 cycles/Å, the power spectrum of BX Mon is dominated by noise. We find $v \sin i = 8.5 \pm 2.0 \ \mathrm{km\,s^{-1}}$. This agrees well with the value found by the direct fitting of weak absorption lines and we retain $v \sin i = 8.5 \pm 2.5 \ \mathrm{km\,s^{-1}}$.

With the photospheric radius R_{r} of the red star, inclination $\sin i = 0.94 \pm 0.06$ and equatorial rotation velocity v, we calculate the rotation period of the M-star as

$$P_{\mathrm{rot}} = \frac{2\pi R_{\mathrm{r}}}{v} = 900 \pm 390 \,\mathrm{days}, \tag{13}$$

with the equatorial rotation velocity

$$v = 9.0 \pm 2.7 \ \mathrm{km\,s^{-1}}. \tag{14}$$

In BX Mon we are facing a system that has an eccentric orbit, co-rotation is therefore not possible. Torques from tidal forces depend strongly on the binary separation (Zahn 1977). Thus in an eccentric orbit the torque will be strongest at periastron passage leading to a rotation period shorter than the orbital period P. This is in agreement with our values.

7. Hα emission line profiles

7.1. Hα line profile observations

Our CAT spectra are not flux calibrated. We used Fe I absorption lines in the underlying M-star continuum in order to scale our Hα spectra to measure the Hα line strength. We assumed that the flux contribution from the M-star is constant in time, but allowed for a variable nebular continuum contribution. This is a reasonable calibration criterion, considering that the available IR magnitudes of BX Mon show no significant variations. This procedure allows us to determine Hα line fluxes on a relative scale. One spectrum cannot be directly scaled, due to the noisy continuum. The Hα equivalent widths and these relative Hα line fluxes are listed in Table 1.

The Hα equivalent widths and line fluxes are strongly reduced at phase $\phi = 0.97$, giving further support to a high inclination i.

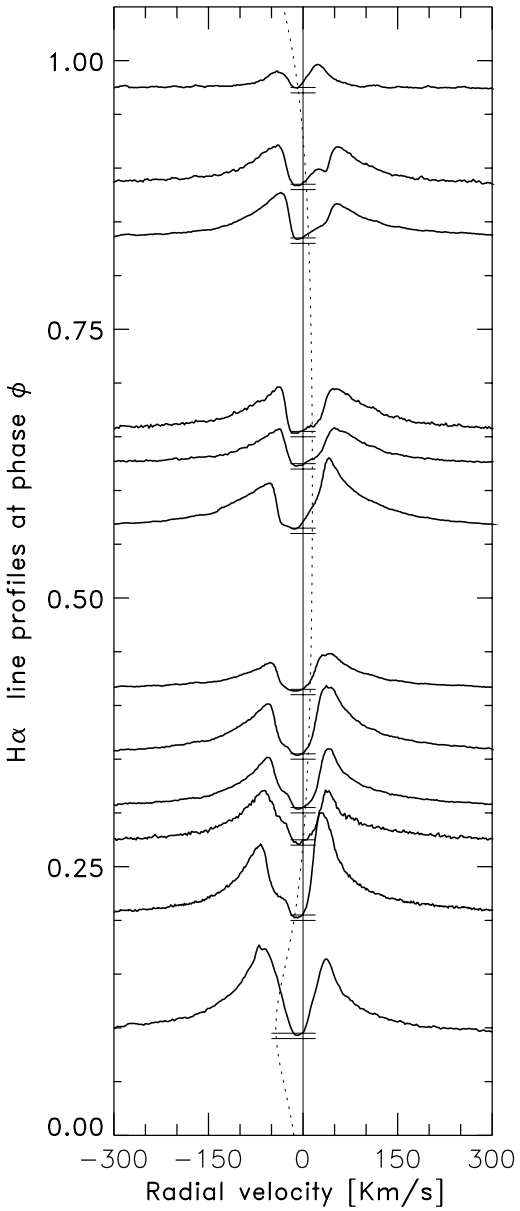

Fig. 9. Normalized Hα line profiles shifted according to their phase ϕ. Velocities are given with respect to the center of mass. The spectrum taken on 12 Sep 1991 ($\phi = 0.27$) has been scaled according to the neighbouring spectra. The short horizontal lines mark the continuum of each spectrum and the zero flux-level. The intersections of the sine-curve (dashed) with the horizontal lines mark the radial velocity of the hot component at the time of observation.

The emission line consists of two principal components. One is a narrow absorption that is approximately at rest with respect to the red giant. It has a full width half maximum (FWHM) of about $50\ \mathrm{km\,s^{-1}}$. The other is a broad emission, with full width at zero intensity of the order of $600\ \mathrm{km\,s^{-1}}$. It is clearly too broad to be due to the undisturbed red giant wind. It may arise from a turbulent zone which is not understood, but it is unlikely to be due to electron scattering or other non-dynamical broadening mechanisms.

7.2. Synthesized Hα profiles

To gain some insight into the origin of the line variations, we have computed a schematic kinematic model of the absorption by the giant wind as a function of orbital phase. The model uses the procedure outlined by Shore et al. (1994). We arbitrarily assume that the absorption is produced by a screen seen against a stable emission line. This focuses attention on the variable column density of the matter in front of the line forming region, while ignoring the problem of formation of the emission line, which is assumed to be formed in the hot gas around the hot component. The absorption line forming region was assumed to be thermodynamically and dynamically decoupled from the ionized region. The only two parameters that are required to produce the observed profile changes are the relative radial velocity of the two stars and the line of sight optical depth toward the emission line producing region. We used a terminal velocity for the red giant wind of $60\ \mathrm{km\,s^{-1}}$. The models are computed assuming an intrinsic Gaussian absorption profile with a FWHM of 2 Å with a turbulent broadening of $v_{\rm turb} = 20\ \mathrm{km\,s^{-1}}$ (Shore & Aufdenberg 1993). Unlike the "iron curtain" models, where column densities and ionization structure were explicitly computed, we used only the velocity gradient and optical depth as the input parameters. The velocity of the red giant wind was specified by:

$$v(r) = v_{\rm turb} + v_\infty(1 - R_r/r)^\beta \qquad (15)$$

where $v_{\rm turb}$ is the turbulent velocity and v_∞ is the terminal velocity for a radial distance r and a stellar radius R_r. For the computation shown in Fig. 10, we employed $\beta = 1$.

One clue to the origin of the absorption component is that it never displays a truly Gaussian profile. The line formed by a simple absorbing wind is always scewed toward the terminal velocity.

At inferior conjunction, the hot component suffers minimum circumstellar extinction and the absorption should be at nearly the terminal velocity, depending on the size of the accelerating region for the wind. At the quadratures, the absorption should extend from the center of mass velocity, V_0, to the terminal velocity, but only on the negative side of the profile in both cases. However, the relative motion of the two components has opposite signs at the two quadratures, so the absorption is shifted with respect to the emission line in opposite directions. At superior conjunction, or eclipse, if the system has a sufficiently high inclination, the absorption should extend over the whole range $[-v_\infty, v_\infty]$ and be at its strongest. The profile should be more flat-bottomed at this phase.

If this picture is correct, it is possible to predict the orbital properties from the profile variations alone. Small relative velocities dominate in the long period, nearly circular systems. Therefore, the absorption line should generally be seen only on the blueward portion of the emission profile. High eccentricity and relatively large radial velocity amplitude can combine to shift the absorption to the red side of the emission peak. Absorption of the red giant continuum may mean one of two things. Either the hot component contributes substantially to the

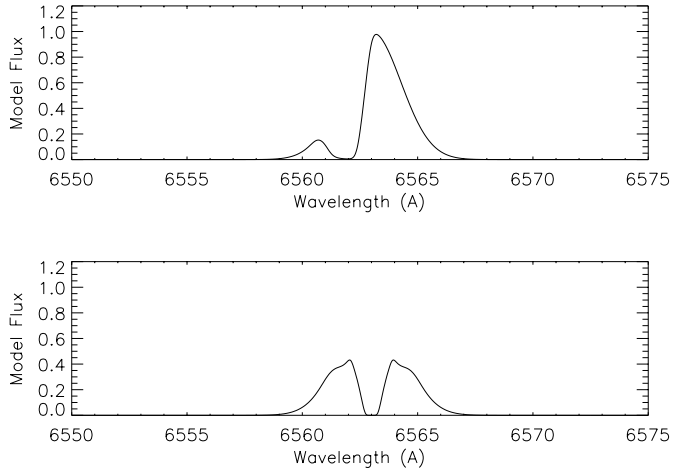

Fig. 10. Synthesized Hα profiles for $\phi = 0.50$ (upper) and $\phi = 0.00$ (lower).

continuum at 6563 Å and the Hα line opacity is great enough to absorb, or the optical depth is always large at that wavelength; this would imply a chromosphere-like layer in the red giant atmosphere. At present, our procedure is too crude to permit detailed modeling of the line formation. But it provides a heuristic guide to the resolution of the origin of the diversity of line profiles observed in the S-type symbiotics. An alternative model based on non-LTE calculations for an expanding red giant's atmosphere ionized from the outside by the radiation of the nearby hot radiation source, can be found in Schwank et al. (1997).

8. Discussion

Normally, only the cool symbiotic component can be observed with optical or near IR spectroscopy and consequently it is only for the cool component that a radial velocity curve can be established. A full description of the binary orbit requires, however, the radial velocities of both stars. Up to now there was only one symbiotic system, AX Per, for which also the hot components' curve was measured. The measurement were possible because during outburst the hot component became accessible to optical observations (Mikolajewska & Kenyon 1992). BX Mon is the second system in which radial velocities of both objects are determined from photospheric absorptions. The spectrum of the hot component in BX Mon is hard to disentangle from the strong and very rich line spectrum of the M giant. We nevertheless succeeded to clearly detect absorption features of the hot component on two occasions near phase $\phi = 0.45$. At that phase, the hot component is located on the observers side and far out in the red giant's wind region (see Fig. 5). Also the maxima in the photographic and visual light curves occur around $\phi = 0.45$ (see Fig. 1c,d) when the contribution of the hot component is at its highest. Thus it is not surprising that we observed the spectrum of the hot component at this phase.

The photographic and visual light curves of BX Mon are far from the typical regular light curve of a binary system. Obscuration of the hot component's light by the outer wind region of the cool giant seems to be particularly important in this system. Thus, the revolving motion of the hot star passing behind the obscuring red giant's wind could explain the shape and the large scatter in the phased light curves and the changing strength of the maxima which are not strictly periodic.

The light curve is completely different in the far UV ($\lambda <$ 2000 Å), where the hot component strongly dominates the emission. There we found a deep eclipse by the cool giant in agreement with our radial velocity curve and the improved orbital period of $P = 1401$ days. The duration of the eclipse is also in agreement with the red giant's radius of $R_r = 160\ \mathrm{R}_\odot$, derived from the spectral type, the apparent magnitude, and the distance. Unfortunately we have no UV observations between phase $\phi = 0.45$ and 0.60, where the maxima in the visual region tend to occur. The presence of long eclipses is an important finding, because it restricts the orbital inclination to $\sin i \geq 0.88$.

From our radial velocity measurements we determined the masses of the stellar components and the orbital configuration. The binary mass-ratio is $q = 6.7 \pm 1.3$, which is somewhat higher than the typical symbiotic value of 3-4 according to Mikolajewska (1997) and Schmid (1998). This is due to the relatively high mass of our red giant ($M_\mathrm{r} = 3.7 \pm 1.9\ \mathrm{M}_\odot$). For the hot component we find $M_\mathrm{h} = 0.55 \pm 0.26\,\mathrm{M}_\odot$. With $e = 0.49$, BX Mon has the highest orbital eccentricity measured in a symbiotic system. The separation between the two components varies between 2.0 and 5.9 AU. At periastron the red giant radius is about 0.6 of the critical Roche radius.

The mass of $M_\mathrm{h} = 0.55\mathrm{M}_\odot$ is an important parameter for clarifying the nature of the hot component in BX Mon. It excludes a main sequence or giant A–F star. The A–F spectrum could be produced by an accretion disk around a low mass main sequence star. However, to power the observed luminosity of the hot component ($L_h \sim 230\ \mathrm{L}_\odot$) such a model requires for a detached system according to Viotti et al. (1986) an uncomfortably high mass accretion rate of $\sim 10^{-4}\,\mathrm{M}_\odot$. The alternative explanation for the hot component is a degenerate (white) dwarf with a hydrogen burning shell. During weak shell flashes, or in a steady state regime where the accreted material is immediately consumed, such a star can reach quite a large radius and a low surface temperature, mimicking an A–F spectrum. Yet, the expected "plateau" luminosity of such an object is $10^3 - 10^4\ \mathrm{L}_\odot$ (Iben & Tutukov 1996), and thus significantly higher than in BX Mon. This, however, is not a fundamental problem, as often in edge-on interacting binaries a luminous compact component is partly or fully hidden by an obscuring material in the orbital plane. We have to admit however, that this argumentation is a easy way out of the hot component's luminosity problem. Further information is needed to establish the exact nature of the hot star in BX Mon.

Advocating that the hot component is a degenerate dwarf, implies that it was initially the primary in the system and thus more massive than $3\,\mathrm{M}_\odot$. It therefore appears that even the more massive progenitors among the known symbiotic systems produce white dwarfs with masses around the canonical value of $M_\mathrm{WD} = 0.6\,\mathrm{M}_\odot$. It is unlikely that objects of such low mass can accrete sufficient material from their present red giant com-

panion to reach the Chandrasekhar limit. This disqualifies symbiotic systems in general as candidates for being progenitors of supernova Type Ia.

BX Mon has a high eccentricity of $e = 0.49$ and a long orbital period of $P = 1401$ days. All other symbiotic systems with well established radial velocity curves also have low eccentricities ($e < 0.1$). These systems have, with the exception of CH Cyg and CD$-43°14303$, shorter orbital periods of $P < 1000$ days. The eccentricity of the orbit for BX Mon is consistent with the circularization time scales of Verbunt & Phinney (1995). Maximum tidal force was excerted while the primary was on the AGB, which would have circularised orbits with periods shorter than 1200 days. This value is a maximum and applies to a primary with initially $3\,M_\odot$. It would be smaller for more massive stars. Thus theory predicts that the binary separation in BX Mon is large enough to escape circularization.

Acknowledgements. We thank the night assistants in Chile and Garching for their fine support for the CAT observations, and the variable star section of the Royal Astronomical Society of New Zealand for providing us with their visual magnitudes. We also wish to thank Dr Janet Mattei for making available Mayall's original photometric data. We are indebted to Hilmar Duerbeck for providing observations in digital form. It is a pleasure to thank Orsola De Marco, Martine Mouchet and Frank Verbunt for fruitful discussions. TD acknowledges financial support by the Swiss National Science Foundation. HMS is supported by the Deutsche Forschungsgemeinschaft (KR 1053/6-1).

References

Allen D.A., 1979, in: Changing Trends in Variable Star Research, F. Bateson et al. (eds), IAU Coll. 46, Univ. Waikato Press, p. 125
Allen D.A., 1982, in: The Nature of Symbiotic Stars, M. Friedjung & R. Viotti (eds) IAU Coll. 70, Reidel, Dordrecht, p. 27
Allen D.A., 1984, Proc. ASA 5, 369
Bessell M.S., Brett J.M., Scholz M., Wood P.R., 1989, A&AS 77, 1
Bidelman W.P., 1954, ApJ Supl.Ser. 1, 175
Brand J., Blitz L., 1993, A&A 275, 67
Dumm T., Schild H., 1998, NewA 3, 137
Dyck H.M., Benson J.A., Van Belle G.T., Ridgway S.T., 1996, AJ 111, Vol.4, 1705
Garcia M.R., 1986, AJ 91, 1400
Gray D.F., 1992, The observation and analysis of stellar photospheres. Cambridge University Press, Cambridge
Iben I., Tutukov A.V., 1996, ApJS 105, 149
Iijma T., 1985, A&A 153, 35
Fanelli, M.N., O'Connell R.W., Burstein D., Wu C.-C., 1992, ApJS 82, 197
Kenyon S.J., 1988, AJ 96, 337
Kukarin, B.V., Parenago, P.P., Efremov, Yu.I., Kholopov, P.N.: 1958, General Catalogue of Variable Stars, The USSR Academy of Science, Moscow
Marcy G.W., Chen G.H., 1992, ApJ 390, 550
Mayall M.W., 1940, Bull. Harvard College Obs. 913,8
Michalitsianos A.G., Kafatos M., Feibelman W.A., Hobbs R.W., 1982, ApJ 253, 735
Mikolajewska J., 1997, in Proceedings of the Conference at Koninki on "Physical Processes in Symbiotic Binaries and related systems", 3
Mikolajewska J., Kenyon S.J., 1992, AJ 103, 579
Munari U.,Iudin B.F., Taranova O.G., Massone G., Marang F., Roberts G., Winkler H., Whitelock P.A., 1992, A&AS 93, 383
Mürset U., Schmid H.M., 1998, to be submitted to A&AS
Neckel T., Klare G., 1980, A&AS 42, 251
Savage D., Mathis J.S., 1979, ARA&A 17, 73
Seaton, M.J., 1979, MNRAS 187, 73
Schild H., Mürset U., Schmutz W., 1996, A&A 306, 477 (Paper II)
Schild H. et al., 1998, in preparation
Schmid H.M., 1998, in Proc. of the 86th meeting of the AAVSO on "Variable stars: New Frontiers", (in press)
Schmid H.M., Dumm T., Mürset U., Nussbaumer N., Schild H., Schmutz W., 1998, A&A 329, 986 (Paper III)
Schmutz W., Schild H., Mürset U., Schmid H.M., 1994, A&A 288, 819 (Paper I)
Schulte-Ladbeck R.E., 1988, A&A 189,97
Schwank M., Schmutz W., Nussbaumer N., 1997, A&A 319, 166
Shore S.N., Aufdenberg J.P., ApJ 416, 355
Shore S.N., Aufdenberg J.P., Michalitianos A.G., 1994 AJ 108, 671
Tsuji T., Ohnaka K., Hinkle K.H., Ridgway S.T., 1994, A&A 289, 469
Verbunt F., Phinney E.S., 1995, A&A 296, 709
Van Winckel H., Duerbeck H.W., Schwarz H.E., 1993, A&AS 102, 401
Viotti R., Altamore M., Ferrari-Toniolo M., Friedjung M., Persi P., Rossi C., Rossi L., 1986, A&A 159, 16
Whitelock P.A., Catchpole R.M., 1983, IBVS 2296
Winfield D. III, Boksenberg A., 1994, The Astronomical Almanac
Zahn J.-P., 1977, A&A 57, 383